Title

Topological graph-based analysis of solid-state ion migration

Permalink

https://escholarship.org/uc/item/62p6x7vn

Journal

npj Computational Materials, 9(1)

ISSN

2057-3960

Authors

Shen, Jimmy-Xuan

Li, Haoming Howard

Rutt, Ann

et al.

Publication Date

2023

DOI

10.1038/s41524-023-01051-2

Copyright Information

Peer reviewed

ARTICLE OPEN

Check for updates

Topological graph-based analysis of solid-state ion migration

Jimmy-Xuan Shen [1,2], Haoming Howard Li [3], Ann Rutt[3], Matthew K. Horton [2,3] and Kristin A. Persson[3,4 ✉]

To accelerate the development of ion conducting materials, we present a general graph-theoretic analysis framework for ion migration in any crystalline structure. The nodes of the graph represent metastable sites of the migrating ion and the edges represent discrete migration events between adjacent sites. Starting from a collection of possible metastable migration sites, the framework assigns a weight to the edges by calculating the individual migration energy barriers between those sites. Connected pathways in the periodic simulation cell corresponding to macroscopic ion migration are identified by searching for the lowest-cost cycle in the periodic migration graph. To exemplify the utility of the framework, we present the automatic analyses of Li migration in different polymorphs of $VO(PO_4)$, with the resulting identification of two distinct crystal structures with simple migration pathways demonstrating overall <300 meV migration barriers.

INTRODUCTION

The migration of charged ions (*eg*. Li, Mg, Na, O^{2-} *etc.*) through solid-state materials is the primary physical mechanism behind the operation of Li-ion batteries, solid-oxide fuel cells, and solid-state electrolytes. Rapid identification and discovery of new materials with favorable migration characteristics is key to developing all-solid-state batteries where the current state-of-the-art organic electrolytes are replaced with a solid-state alternative, leading to improved power density and safety. Traditionally, the discovery of electrode materials has focused on compounds that contain the migrating ion in their as-synthesized state. However, this is not a strict requirement, and many materials synthesized without the migrating species are capable ion conductors. In fact, it has been shown that for multivalent applications, materials that are synthesized without the working ion tend to exhibit a flatter migration energy landscape and hence better performance[1–4].

The established method for identifying the optimal path between two sites in a crystal is the nudged-elastic band (NEB) method[5,6]. However, NEB calculations are computationally costly and are only able to analyze short-distance migration events provided that an initial, reasonably accurate, guess for the connecting path is available. To understand the migration characteristics of a material, the motion of the ion through the entire crystal must be considered. Recent high-throughput studies have attempted to address this either by simplifying the problem to analyzing the migration of a single working ion particle in a fictitious field[7] or by focusing on individual migration events but not how they connect over larger distances[8]. Additionally, previous work exclusively treat materials where valid sites for the working ion are known beforehand. To explore the broader class of materials, where there is no a priori knowledge of the sites and migration properties of the possible intercalants, it is of considerable interest to develop algorithms and frameworks to analyze possible ion migration behavior in any crystalline solid.

In this endeavor, we employ a recently developed methodology where the charge density-analysis was shown to be a reliable descriptor for generating initial guesses of working ion sites[9]

which allows us to systematically identify metastable intercalation sites in any crystalline structure. Here, we build upon this framework and present a graph theory extension to automatically identify ion migration pathways in any periodic solid. The migration is treated as a periodic graph where symmetrically equivalent copies of the metastable sites constitute the nodes and the individual migration events between these sites are the edges. Additionally, we assign a cost to the graph edges based on the migration energy barriers and showcase how optimal intercalation pathways can be discovered with a Dijkstra's-inspired algorithm defined on the periodic graph. The original code provided here is distributed as an extension to the `pymatgen` material analysis library. We demonstrate our framework on two well-known structures of MnO_2 and CoO_2 to show how the migration graphs can be constructed and utilized. Finally, the methodology is applied to the different configurations of $VO(PO)_4$ in the Materials Project[10] to assess the migration characteristics of each poly-morph, and we exemplify the capability to identify promising new ionic conductors within this set of materials.

RESULTS & DISCUSSIONS

Site identification

Our graph-based migration analysis is best suited for the two limits of working ion occupation, either single-ion migration in the dilute limit or vacancy migration in the fully intercalated limit. While it is possible to analyze intermediate concentrations, the large configurational space associated with the working ion ordering arrangements make a thorough investigation computa-tionally demanding and not suitable for high-throughput evalua-tion of viable intercalation pathways. For vacancy migration, a priori knowledge of the working ion sites makes the construction of migration graphs trivial. In materials where we lack knowledge of working ion sites, we utilize a recently developed, generally robust computational workflow for identifying the metastable sites of the working ion in any structure[9]. The methodology selects candidate sites at the local minima of charge density and, for each candidate site, a working ion is inserted and the structure is

[1]Materials Science Division, Lawrence Livermore National Laboratory, Livermore, CA, USA. [2]Materials Sciences Division, Lawrence Berkeley National Laboratory, Berkeley, USA. [3]Department of Material Science and Engineering, University of California, Berkeley, CA, USA. [4]Molecular Foundry, Lawrence Berkeley National Laboratory, Berkeley, USA. ✉email: kapersson@lbl.gov

npj
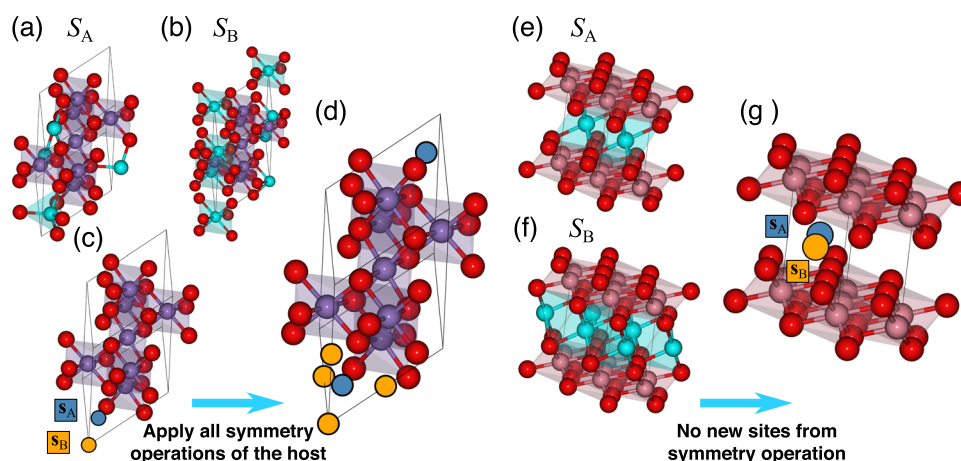
Fig. 1 Illustration of identified metastable sites in MnO2 and CoO2. a, b Crystal structure indicating the different relaxed atomic structures of MnO2 after single Li insertion. **e, f** Crystal structure indicating the different relaxed atomic structures of CoO2 after single Li insertion. **c** Crystal structure indicating the metastable Li position after mapping onto S_{base}. **d, g** Crystal structure with the full set of possible Li sites after symmetry operations. Note that the applied symmetry operations did not result in additional sites for CoO2.

allowed to relax using density-functional theory calculations. An inserted structure is considered "topotactic" if the positions of its framework atoms closely resemble the relaxed atomic positions of the host material. The metastable sites are obtained by mapping the working ion in the topotactically inserted structures onto the empty host structure and identifying all symmetry-equivalent positions in the host structure. Based on the location and connectivity of the metastable sites, we build our graph-based migration analyses.

To exemplify our approach, we use two materials: MnO2_2 in the λ phase[11] with cubic spinel structure and layered CoO2 with ABBA stacking[12]. After performing indepedent single Li insertions into the sites suggested by the charge density analysis and relaxing the new structures[9], two distinct singly-inserted structures for each material were topotactically matched to the host material as shown in Fig. 1. We denote the base structure S_{base} and the set of relaxed inserted topotactic structures $\{S_\alpha\}$ where $\alpha \in \{A, B\}$ for both examples. Since the host sublattice (which does not contain the working ion) of each S_α can be mapped onto S_{base}, the relaxed positions of the cations in each structure can also be mapped to position s_α in S_{base}. This mapping allows us the identify two symmetry-distinct metastable sites s_A (blue) and s_B (orange) for MnO2 and CoO2, respectively. Utilizing the `spglib` package[13] and its interface with `pymatgen`[14], we analyze the crystal symmetry of the structure with the inserted ion, S_{base}, and apply the valid point group operations to each s_α to generate all of the possible cation positions, designated by an integer index value i at position r_i, in the unit cell.

In MnO2, the s_A metastable site is represented by the fractional coordinates $(\frac{1}{8}, \frac{1}{8}, \frac{1}{8})$ and all space-group operations of the host material will either map the site to itself or $(\frac{7}{8}, \frac{7}{8}, \frac{7}{8})$. The s_B site is represented by the fractional coordinates $(0, 0, 0)$, which has three additional symmetry-equivalent sites as shown in Table 1. This results in a total of six metastable sites per unit cell as shown in Fig. 1d. We perform the same analysis for CoO2, which results in s_A and s_B at the face centers of the primitive cell. The space-group operations of CoO2 map the sites onto periodic images of the original, as such, no new symmetrically equivalent sites are created from symmetry operations, the resulting two metastable sties are shown in Fig. 1g.

We can see how the charge-density based site identification performs across a wide range of structures and intercalating ion types by examining the distributions of the distances between the charge-density local minima and the nearest metastable sites. To accomplish this, we queried the Materials Project database for Li,

Mg, and Ca cathode materials where the fully-charged entry does not contain the intercalating species. To keep the numbers of entries for each ion type comparable, we limit the Li search to entries where the host material's decomposition energy (energy above convex hull) is less than 0.01 eV/atom, compared to 0.1 eV/atom for Mg and Ca. This resulted in 196 battery materials for Li, 145 for Mg, and 111 for Ca. For these materials we examined the topotactically matched structure in the Materials Project database with the lowest fraction of the inserted ion to obtain a set of metastable insertion sites. The distribution of the distances between between these metastable sites and the nearest local minimum in the charge-density is shown in Fig. 2 where the distributions for the different inserted species are stacked on top of each other. From this, we see that Mg and Ca ion insertions exhibits better performance for insertion algorithm. For the larger cations (Mg, Ca), the insertion algorithm is able to guess within 1 Å of the metastable site in the overwhelming majority of cases. For Li, since the insertion cavity can be much larger than the Li ion, the ion can relax to a position that is further from the initial guess once charge is exchanged between Li and the host structure. However, this degree of ionic relaxation should not be problematic for the ionic relaxation algorithms in modern DFT codes.

Graph analysis

Using a distance cutoff of l_{max}, we connect two nearby metastable sites r_i and r_j to represent a discrete migration event in the material which we will call a "hop". The network formed by these hops is infinite and the following convention ensures that we only consider hops that are inequivalent by lattice transitions. Each hop between sites i and j in the periodic unit cell is labeled $h_{ij}^{\mathbf{K}}$ where the additional index $\mathbf{K}$ is an integer-valued vector representing the relative periodic image displacement between the endpoints [ie. $\mathbf{K} = (0, 0, 1)$ means that the hop crosses a period cell boundary once in the positive c-direction]. In general, we consider the migration graph to be undirected. As such, the hops $h_{ij}^{\mathbf{K}}$ and $h_{ji}^{-\mathbf{K}}$ will represent the same migration event, but only one representation will be present in the graph. As a convention to prevent double-counting, we require the site indices to satisfy $i \leq j$. Additionally, since there is ambiguity when $j = i$ and $\mathbf{K} \neq 0$, we only retain the hop where the first non-zero component of $\mathbf{K}$ is positive.

Using a threshold value of $l_{max} = 3$ Å, the migration graph for Li^+ in MnO2 (denoted as $\mathcal{G}(MnO_2)$) is constructed and shown in Fig. 3a, b. There are 18 hops in $\mathcal{G}(MnO_2)$ that are not equivalent under discrete lattice translations. Using the space group

Table 1. Space group mapping of Li positions s_i in MnO_2 under the space group operations host crystal structure.

Index	Label	Original position	Host transformations[a]	Transformed position
0	s_A	$(\frac{1}{8}, \frac{1}{8}, \frac{1}{8})$	(x, y, z), $(z, -x-y-z+\frac{1}{2}, x)$ $(-x-y-z+\frac{1}{2}, z, y)$, $(y, x, -x-y-z+\frac{1}{2})$ $(y, z, -x-y-z+\frac{1}{2})$, $(-x-y-z+\frac{1}{2}, x, y)$ (z, y, x), $(x, -x-y-z+\frac{1}{2}, z)$	$(\frac{1}{8}, \frac{1}{8}, \frac{1}{8})$
1	s_A	$(\frac{1}{8}, \frac{1}{8}, \frac{1}{8})$	$(-y, -z, x+y+z+\frac{1}{2})$, $(x+y+z+\frac{1}{2}, -x, -y)$ $(-z, -y, -x)$, $(-x, x+y+z+\frac{1}{2}, -z)$ $(-x, -y, -z)$, $(-z, x+y+z+\frac{1}{2}, -x)$ $(x+y+z+\frac{1}{2}, -z, -y)$, $(-y, -x, x+y+z+\frac{1}{2})$	$(\frac{7}{8}, \frac{7}{8}, \frac{7}{8})$
4	s_B	$(0, 0, 0)$	(x, y, z), $(-z, -y, -x)$, $(-x, -y, -z)$, (z, y, x)	$(0, 0, 0)$
3	s_B	$(0, 0, 0)$	$(x+y+z+\frac{1}{2}, -x, -y)$, $(-x-y-z+\frac{1}{2}, z, y)$ $(-x-y-z+\frac{1}{2}, x, y)$, $(x+y+z+\frac{1}{2}, -z, -y)$	$(\frac{1}{2}, 0, 0)$
2	s_B	$(0, 0, 0)$	$(z, -x-y-z+\frac{1}{2}, x)$, $(-x, x+y+z+\frac{1}{2}, -z)$ $(-z, x+y+z+\frac{1}{2}, -x)$, $(x, -x-y-z+\frac{1}{2}, z)$	$(0, \frac{1}{2}, 0)$
5	s_B	$(0, 0, 0)$	$(-y, -z, x+y+z+\frac{1}{2})$, $(y, x, -x-y-z+\frac{1}{2})$, $(y, z, -x-y-z+\frac{1}{2})$, $(-y, -x, x+y+z+\frac{1}{2})$	$(0, 0, \frac{1}{2})$

[a]Determined by the `SpacegroupAnalyzer`.
The positions of the s_i's and their images are given in fractional coordinates.
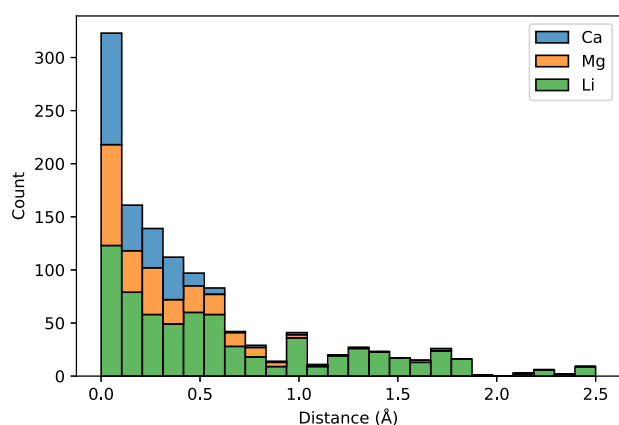
Fig. 2 Distribution of cation insertion position errors. Stacked histograms of the distribution of the distances between the nearest local minimum in the charge-density and the metastable site obtained from symmetry mapping of topotactically matched structures for Li, Mg, and Ca.

symmetry between the hops, we can reduce them to 2 symmetry-distinct groups indicated by the edge color in the graph. The Li^+ migration graph in CoO_2, with 8 hops in 3 symmetry-distinct groups, is shown in Fig. 3c, d. For a complete enumeration of the migration hops in these two materials and their symmetry equivalence, see Supplementary Table 2 and 3 in the Supplementary Information[15]. In principle, once we have identified the symmetrically equivalent groups, we can obtain the migration barrier using NEB calculations[6] to chart the migration energy landscape of the material.

A candidate ion-conducting material must enable a continuous migration pathway for the working ion across the unit cell, connecting to the next one. In a periodic system, continuous pathways are infinite, which we term "intercalating pathways". Since our migration graph contains only one copy of each node, periodicity manifests via the image displacement vector $\mathbf{K}$. The intercalating pathways are essentially cycles in the graph where
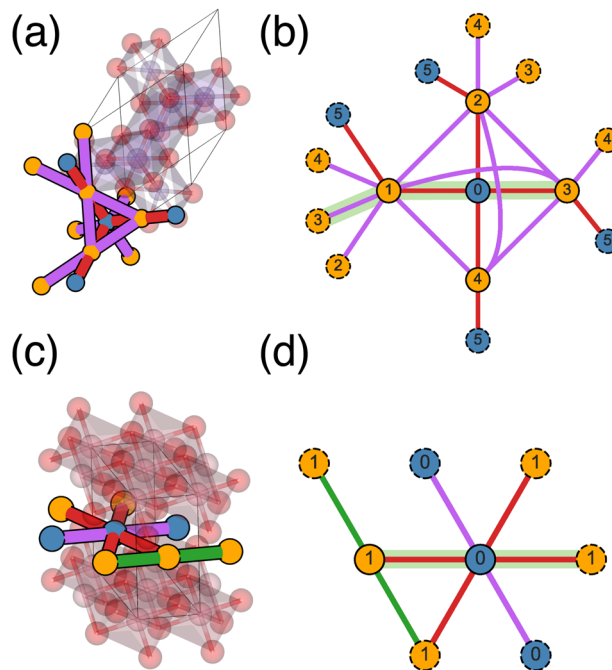
Fig. 3 Graph representation of the migration hops in MnO_2 and CoO_2. a, c Crystal structures of MnO_2 (**a**) and CoO_2 (**c**) with hops shown that fall below 3 Å and are colored by symmetric equivalence. **b, d** The migration graphs for the two materials MnO_2 (**b**) and CoO_2 (**d**) are shown, where dashed nodes represent j-index nodes that are outside the (0,0,0) unit cell. Although there is only one periodic copy of each node, the dashed nodes are used to differentiate the multiple edges connecting the same two nodes. Two examples of intercalating pathways are highlighted in light green in (**b, d**).

the total image displacement is non-zero. The series of hops in such a cycle will connect a metastable site to a different periodic image of itself, which constitutes a repeating unit of an infinite periodic migration pathway. Basic examples of intercalating

pathways are highlighted in light green in Fig. 3b, d which connect a node to a periodic image of itself. To identify these pathways, we used a modified Dijkstra's type algorithm on the periodic graph. The key difference between the modified algorithm and the original Dijkstra's algorithm is that the periodic image vector is tracked during graph traversal. This means that the optimal cost to reach any node during the graph traversal is defined for the combination of node index i and periodic image vector $\mathbf{K}$. A detailed description of the path-finding algorithm on the periodic graph is presented in the SI (Supplementary Algo. 1). The cost function employed in the path-finding algorithm can be any positive definite function assigned to the edges of the graph. A good choice in most cases is the migration energy barrier (defined as the maximum difference between the NEB energy and the linear interpolation between the site energies) for the ion-migration event represented by that particular edge. However, the difference between the binding energies of the endpoints, which can be computed without expensive NEB calculations, may also be used as a lower bound of the activation barrier for screening purposes.

Application to polymorphs of VO(PO$_4$)

We demonstrate the utility of the obtained migration graphs for Li migration in VO(PO$_4$). Of all 18 VO(PO$_4$) phases currently available in the Materials Project, five are distinct known, synthesized phases with the following IDs(spacegroup symbols): mp-25265(Pnma), mp-556459(Cc), mp-559299(P4/n), mp-763482(P4/n), mp-1104567(C2/m). While all five phases listed above have been experimentally synthesized, only some of them have readily available electrochemical analysis data. In particular, mp-25265 (β-VOPO$_4$) demonstrates a capacity of 118.6 mAh/g against Li insertion at average 4 V[15], and mp-556459 (ε-VOPO$_4$) has shown a capacity of 305 mAh/g against Li insertion over two voltage plateaus at about 4.0 and 2.5 V[16]. For each of the five structures, we performed a set of ion insertions to generate metastable sites and constructed the migration graphs, yielding connectivity of hops to form intercalation pathways. With the connectivity of the graph established, the only missing piece to a complete description of the intercalation behavior is understanding of the ion migration energy evolution during the individual hops.

The energy profile for each hop can be estimated by utilizing the ApproxNEB method[17] in `atomate`. The ApproxNEB method performs independent constrained optimizations for each image structures which allows us to trade accuracy for speed since the independent relaxations are trivially parallelised. Each phase of VO(PO$_4$) has 3 to 10 such hops and thus 3 to 10 ApproxNEB calculations. Due to the high computational cost involved, one might find it helpful, in general, to rank migration pathways before ApproxNEB is employed. To demonstrate testing of one possible choice of cost function for this purpose, we performed charge-density analyses on these phases and compared them to our ApproxNEB results.

We examined the total change-density in a radius 1 Å cylinder between sites the end points of a hop; $\rho_{cyl}(h_{ij}^{\mathbf{K}})$. Since the background charge density can change between different structures, we will only focus on the *relative charge barrier*, defined as the ratio between the integrated charge, $\rho_{cyl}(h_{ij}^{\mathbf{K}})$, and its minimum value in that particular structure; $\min(\rho_{cyl}(h_{ij}^{\mathbf{K}}))$. The relationship between the total charge ratio and the ApproxNEB barrier is shown in Fig. 4c, which indicates little correlation between the total charge in the cylinder and the energy barrier. Hence, while promising insertion sites could be identified by low charge-density, it is clear that local atomic relaxations around the working ion during the migration significantly impact the energy barrier such that those effects cannot be ignored. However, since the relative charge barrier is an indicator of the amount of negative charge that the migrating ion has to move through we
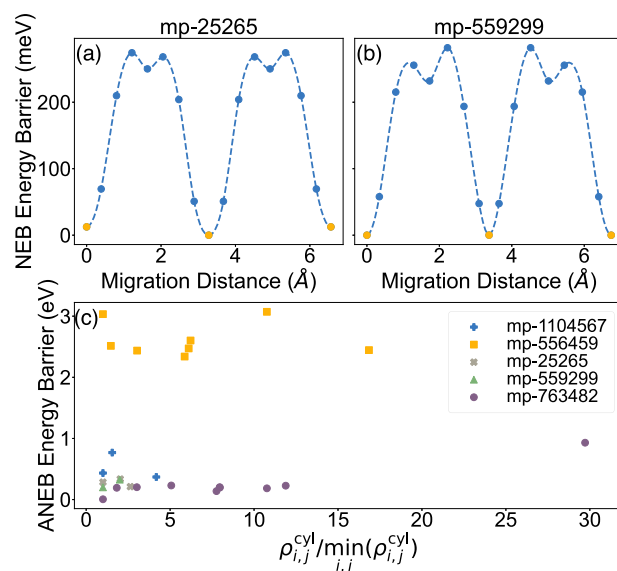
Fig. 4   Periodic migration energy landscapes for VO(PO$_4$). a, b The NEB-calculated energy landscapes along the lowest-barrier paths for mp-25265 (**a**) and mp-559299 (**b**) are shown. These two optimal paths both contain 2 hops. **c** Comparison between the ApproxNEB energy barriers vs. the relative charge barrier $[\rho_{cyl}(h_{ij}^{\mathbf{K}}) / \min \rho_{cyl}(h_{mn}^{\mathbf{K}})]$ of all the hops in the five chosen phases of VO(PO$_4$).

are most interested in migration evens with low relative charge and low ApproxNEB barriers, i.e. the bottom left corner of Fig. 4c, for further analysis using ApproxNEB.

With details of the hops and their connectivity, we can now construct a complete picture of long-range migration in the system. In Figure 4a, b, we show the lowest energy barrier intercalation pathway for two of the structures (mp-25265 and mp-559299) that contain multiple low-barrier hops. In order to reach an accurate description, we performed NEB calculations when evaluating the energy landscape of each hop, the results of which show that both structures contain an intercalation pathway which has an overall energy barrier of less than 250 eV.

Discussions

We demonstrate that the intercalation properties of cations in a solid-state material can be fully captured by a migration graph where the metastable sites represent the nodes and the migration energy barriers are the edge weights. Using a previously-developed, unbiased cation insertion algorithm, we identify the symmetry-distinct metastable sites in the structure and generate all equivalent sites by repeatedly applying the symmetry operations of the host. The migration energy is calculated for the symmetrically-distinct hop between pairs of adjacent meta-stable sites and the data is replicated on symmetrically equivalent hops to obtain the migration barriers on the entire graph. To identify intercalating pathways, we detect cycles in the periodic graph. Finally, we applied this analysis framework on a diverse set of polymorph structures of VO(PO$_4$) and present several promising structures with low migration barriers. The framework and code presented here can be used to automatically obtain the migration properties of solid-state materials with essentially no a priori knowledge. Our work opens up opportunities for high throughput studies in the future and can offer a deeper understanding of the migration properties of crystalline solids. Compared with the single-particle charge-density models by Kahle et al.[7,18], our method will typically be slower but will capture more of the quantum effects in the system since we are using NEB to analyze the discrete migration events. Since we have also developed a

flexible charge-density API[19], we can combined these methods for future high-throughput studies.

Since this methodology relies on identification of the metastable sites, we will need to continue filling in under-explored regions of the chemical space in the Materials Project database to study migration at scale. Additionally, while our prior work[9] addressed the process of identifying metastable sites to increase cation incorporation, the current work only considers the migration properties in the dilute and vacancy limits. In the future, we will need to extend the analysis to away from the dilute and vacancy limits to capture the migration characteristics for more realistic systems.

METHODS

The total energy of each atomic structure was calculated from first principles using density-functional theory with the generalized-gradient approximation (GGA) functional of Perdew-Burke-Ernzerhof (PBE) implemented in the Vienna Ab initio Simulation Package (VASP). The Hubbard U values for Co, Mn, and V were set to 3.32, 3.90, and 3.25 eV, respectively.

DATA AVAILABILITY

The data that support the findings of this study are available on the Materials Project website (`materialsproject.org`)

CODE AVAILABILITY

The code for the metastable site analysis and graph analysis is available as part of the `pymatgen-analysis-diffusion` namespace package which acts as an add-on to the main `pymatgen` library.

REFERENCES

1. Kim, S. et al. High-voltage phosphate cathodes for rechargeable Ca-ion batteries. *ACS Energy Lett.* **5**, 3203–3211 (2020).
2. Sun, X., Bonnick, P. & Nazar, L. F. Layered TiS$_2$ positive electrode for Mg batteries. *ACS Energy Lett.* **1**, 297–301 (2016).
3. Rong, Z. et al. Materials Design Rules for Multivalent Ion Mobility in Intercalation Structures. *Chem. Mater.* **27**, 6016–6021 (2015).
4. Levi, E. & Aurbach, D. Chevrel Phases, MxMo6T8 (M = Metals, T = S, Se, Te) as a Structural Chameleon: Changes in the Rhombohedral Framework and Triclinic Distortion. *Chem. Mater.* **22**, 3678–3692 (2010).
5. Mills, G. & Jónsson, H. Quantum and thermal effects in H$_2$ dissociative adsorption: Evaluation of free energy barriers in multidimensional quantum systems. *Phys. Rev. Lett.* **72**, 1124–1127 (1994).
6. Jónsson, H., Mills, G. & Jacobsen, K. W. Nudged elastic band method for finding minimum energy paths of transitions. *cqdc*385-404 (1998).
7. Kahle, L., Marcolongo, A. & Marzari, N. High-throughput computational screening for solid-state Li-ion conductors. *Energy Environ. Sci.* (2020).
8. Bölle, F. T. et al. Autonomous discovery of materials for intercalation electrodes. *Batteries Supercaps* **3**, 488–498 (2020).
9. Shen, J.-X., Horton, M. & Persson, K. A. A charge-density-based general cation insertion algorithm for generating new Li-ion cathode materials. *npj Comput. Mater.* **6** (2020).
10. Jain, A. et al. Commentary: The materials project: a materials genome approach to accelerating materials innovation. *APL Mater.* **1**, 011002 (2013).
11. Juran, T., Young, J. & Smeu, M. Density functional theory modeling of MnO$_2$ polymorphs as cathodes for multivalent ion batteries. *J. Phys. Chem. C.* **122**, 8788–8795 (2018).
12. Laubach, S. et al. Changes in the crystal and electronic structure of LiCoO$_2$ and LiNiO$_2$ upon Li intercalation and de-intercalation. *Phys. Chem. Chem. Phys.* **11**, 3278–3289 (2009).
13. Togo, A. & Tanaka, I. Spglib: a software library for crystal symmetry search. *arXiv*https://arxiv.org/abs/1808.01590 (2018). 1808.01590.
14. Ong, S. P. et al. The Materials Application Programming Interface (API): a simple, flexible and efficient API for materials data based on REpresentational State Transfer (REST) principles. *Comput. Mater. Sci.* **97**, 209–215 (2015).
15. Ren, M. M., Zhou, Z., Su, L. W. & Gao, X. P. LiVOPO4: A cathode material for 4V lithium ion batteries. *J. Power Sources* **189**, 786–789 (2009).
16. Siu, C. et al. Enabling multi-electron reaction of ϵ-VOPO 4 to reach theoretical capacity for lithium-ion batteries. *Chem. Commun.* **54**, 7802–7805 (2018).
17. Rong, Z., Kitchaev, D., Canepa, P., Huang, W. & Ceder, G. An efficient algorithm for finding the minimum energy path for cation migration in ionic materials. *J. Chem. Phys.* **145**, 074112 (2016).
18. Kahle, L., Marcolongo, A. & Marzari, N. Modeling lithium-ion solid-state electrolytes with a pinball model. *Phys. Rev. Mater.* **2**, 065405 (2018).
19. Shen, J.-X. et al. A representation-independent electronic charge density database for crystalline materials. *Sci. Data* **9**, 1–7 (2022).

AUTHOR CONTRIBUTIONS

J.X.S. developed the site-mapping and graph algorithms and performed the calculations on the example MnO$_2$ and CoO$_2$ systems; H.H.L. performed the ApproxNEB and NEB calculations for the VO(PO$_4$) systems, A.R. developed the automated workflow to perform the ApproxNEB calculations; M.K.H. contributed design ideas and support at all stages of the algorithm development; K.A.P provided supervision and funding for the project at all stages. All authors contributed significantly to the preparation of this manuscript.

COMPETING INTERESTS

The authors declare no competing financial or non-financial interests.

ADDITIONAL INFORMATION

Supplementary information The online version contains supplementary material available at https://doi.org/10.1038/s41524-023-01051-2.

Correspondence and requests for materials should be addressed to Kristin A. Persson.

Reprints and permission information is available at http://www.nature.com/reprints

Publisher's note Springer Nature remains neutral with regard to jurisdictional claims in published maps and institutional affiliations.